



1 **Effectiveness of Emission Controls on Atmospheric Oxidation**
2 **and Air Pollutant Concentrations: Uncertainties due to Chemical**
3 **Mechanisms and Inventories**

4

5 Mingjie Kang^{1,2}, Hongliang Zhang³, Qi Ying^{4,a}

6

7 ¹ School of Applied Meteorology, Nanjing University of Information Science and
8 Technology. Nanjing 210044, China.

9 ² Atmospheric Environment Center, Joint Laboratory for International Cooperation on
10 Climate and Environmental Change, Ministry of Education, Nanjing University of
11 Information Science and Technology. Nanjing 210044, China.

12 ³ Department of Environmental Science and Engineering, Fudan University, Shanghai
13 200433, China.

14 ⁴ Zachry Department of Civil and Environmental Engineering, Texas A&M University,
15 College Station, Texas 77843-3136, USA.

16 ^a Currently at the Division of Environment and Sustainability, Hong Kong University of
17 Science and Technology, Clear Water Bay, Kowloon, Hong Kong, China.

18

19 *Correspondence to:* Qi Ying (qying@ust.edu)



20 **Abstract.** In this study, three photochemical mechanisms of varying complexity from the
21 Statewide Air Pollution Research Center (SAPRC) family and two widely used anthropogenic
22 emission inventories are employed to quantify the discrepancies in the predicted effectiveness
23 of nitrogen oxides (NO_x) and volatile organic compound (VOC) emission controls on ozone
24 (O_3), secondary inorganic aerosols (SIA), and hydroxyl (OH) and nitrate (NO_3) radicals using
25 the Community Multiscale Air Quality (CMAQ) model. For maximum daily average 8-hour
26 O_3 (O_3 -8h), relative reductions predicted using different emission inventory and mechanism
27 combinations are consistent for up to 80% NO_x or VOC reductions, with maximum differences
28 of approximately 15%. For secondary inorganic aerosols (SIA), while the predicted relative
29 changes in their daily average concentrations due to NO_x reductions are quite similar, very
30 large differences of up to 30% occur for VOC reductions. Sometimes even the direction of
31 change (i.e., increase or decrease) is different. For the oxidants OH and NO_3 radicals, the
32 uncertainties in the relative changes due to emission changes are even larger among different
33 inventory-mechanism combinations, sometimes by as much as 200%. Our results suggest that
34 while the O_3 -8h responses to emission changes are not sensitive to the choice of chemical
35 mechanism and emission inventories, using a single model and mechanism to evaluate the
36 effectiveness of emission controls on SIA and atmospheric oxidation capacity may have large
37 errors. For these species, the evaluation of the control strategies may require an ensemble
38 approach with multiple inventories and mechanisms.



39 **1. Introduction**

40 Tropospheric ozone (O_3) pollution remains a major global concern. O_3 plays a critical role in
41 atmospheric chemistry and is an important target for air quality improvement (Lu et al., 2018;
42 Lyu et al., 2023; Real et al., 2024) because high levels of surface O_3 negatively affect human
43 health, agricultural crop yields and plant growth (Du et al., 2024; Feng et al., 2022; Ghude et
44 al., 2016; Lu et al., 2020; West et al., 2006). Surface O_3 is mainly formed by the photochemical
45 reactions of NO_x and volatile organic compounds (VOCs) emitted from anthropogenic and
46 biogenic sources (Finlayson-Pitts and Pitts Jr, 1999; Seinfeld and Pandis, 2016). The
47 development of effective O_3 control strategies is hampered by the considerable spatial and
48 temporal variability of surface O_3 concentrations and their non-linear relationship with
49 emissions and meteorological conditions.

50 Three-dimensional chemical transport models (CTMs) are a valuable tool for developing
51 effective air pollution control strategies. They can provide spatial and temporal information on
52 O_3 , particulate matter, and toxic air pollutants by numerically solving the mathematical
53 equations describing the emission, reaction, transport, and deposition of primary and secondary
54 atmospheric pollutants (Byun and Schere, 2006; Russell, 1997). The veracity of modeling
55 outcomes is contingent upon the gas-phase chemical mechanisms and emission inventories,
56 among other variables. Reliance on a single chemical mechanism and emission inventory may
57 result in substantial uncertainty in modelled pollutant concentrations. A common approach to
58 reduce uncertainty in air quality model predictions is to use an ensemble of simulations with
59 different emission inventories and chemical mechanisms (Hu et al., 2017a).

60 Photochemical mechanism is one of the core components of all CTMs. While the
61 representation of inorganic chemistry is generally similar across mechanisms, the
62 representation of atmospheric organic chemistry differs significantly in terms of the number of
63 explicit model species, the lumping schemes, and the radical chemistry, leading to variations
64 in the model predictions of O_3 , $PM_{2.5}$, air toxics, and some important radical species (Griffith
65 et al., 2016; Kim et al., 2009). Furthermore, the responses of the predictions to changes in
66 emissions may also differ depending on the photochemical mechanism employed, which may
67 impact the assessment of emission control strategies. In practical applications, it is of the
68 utmost importance to strike a balance between mechanism complexity and computational
69 efficiency. For long-term modeling studies of criteria pollutants and the evaluation of
70 numerous emission control strategies, condensed mechanisms may prove to be the optimal
71 choice. More detailed mechanisms are appropriate for a broader range of applications, such as



72 investigations into specific reaction products that are not explicitly represented in condensed
73 mechanisms. However, they are more demanding on computational resources.

74 In this context, several mechanism comparison studies have been conducted. Differences
75 in predicted O₃ levels using various photochemical mechanisms have been reported (Yu et al.,
76 2010; Venecek et al., 2018). In addition to directly comparing the model predictions of O₃
77 concentrations, comparative analyses were also undertaken to examine the similarities and
78 differences between these mechanisms in predicting O₃ changes in response to changes in
79 precursor emissions. For example, Li et al. (2012) and Kang et al. (2022) compared several
80 mechanisms from the SAPRC family, including the standard versions of SAPRC-99, SAPRC-
81 07, SAPRC-11, and a highly condensed version of SAPRC-07. Their results showed that,
82 despite discrepancies in the predictions for O₃, key radicals such as OH and HO₂, and oxidation
83 products such as HNO₃, H₂O₂, NO₂, PAN, and HCHO, the relative changes in O₃ due to
84 changes in NO_x and VOC emissions were almost identical.

85 On the other hand, the accuracy of model predictions is also significantly affected by
86 uncertainties in anthropogenic emission inventories (Hu et al., 2017a; Kang et al., 2022; Placet
87 et al., 2000), which primarily arise from uncertainties and variability in activity levels (e.g.,
88 industrial production or energy consumption) and emission factors (Akimoto et al., 2006; Lei
89 et al., 2011; Streets et al., 2003). For example, when local speciation profiles are not available
90 for the generation of mechanism-specific VOC emissions from the emission rate of non-
91 methane hydrocarbons, average speciation profiles from the SPECIATE database developed
92 by the US EPA were often adopted (Bray et al., 2019; Li et al., 2014; Streets et al., 2003; Wu
93 and Xie, 2017). However, the emission factors from the SPECIATE profiles are predominantly
94 representative of the characteristics of local emissions, as a consequence of the disparities in
95 emission standards and control technologies among diverse geographical regions (Sha et al.,
96 2021). This introduces uncertainties into the emissions and the predicted pollutant
97 concentrations.

98 To date, several emission inventories covering China have been developed, such as the
99 Multi-resolution Emission Inventory for China (MEIC), the Regional Emission inventory in
100 ASia (REAS), and the Emission Database for Global Atmospheric Research (EDGAR). These
101 inventories have been successfully applied in chemical transport modeling to investigate the
102 concentration and spatial distribution of O₃ and other pollutants (Hu et al., 2017b; Kang et al.,
103 2021; Li et al., 2019, 2018; Saikawa et al., 2017; Xue et al., 2020; Yamaji et al., 2008). Hu et
104 al. (2017a) reported inconsistencies in emission inventories in predicting O₃ and PM_{2.5} using
105 the Weather Research and Forecasting/Community Multiscale Air Quality (WRF/CMAQ)



106 model system. Ma et al. (2004) identified variations in NO_x and VOC emissions among
107 different inventories as the main factors influencing modeled O_3 concentrations. Our previous
108 study, which employed the condensed SAPRC-07 mechanism and two anthropogenic emission
109 inventories (MEIC and REAS), also observed relatively larger differences in O_3 predictions
110 between inventories in megacities of Beijing and Shanghai, especially on days with elevated
111 O_3 levels (Kang et al., 2022).

112 While several studies have explored the differences in model predictions due to varying
113 chemical mechanisms or emission inventories, a comprehensive analysis of the influence of
114 diverse combinations of these two factors on the sensitivity of O_3 and other air pollutants to
115 emission changes in China has yet to be undertaken. In this study, we address this gap by
116 applying the CMAQ model, integrated with three photochemical mechanisms and two widely
117 used emission inventories, to quantify the effects of different combinations of mechanisms and
118 inventories on the predictions of maximum daily average 8-hour ozone (O_3 -8h) and other
119 secondary pollutants in different regions of China. In addition, the impacts on atmospheric
120 oxidation capacity and key gaseous pollutants are investigated. To gain insight into the
121 variations in pollutant sensitivity, a series of incremental emission reduction scenarios were
122 used, thereby enabling the quantification of the influence of different mechanism and inventory
123 combinations on the response of O_3 and related pollutants. The findings of this study can assist
124 policymakers in the development of more effective and adaptive pollution control strategies.

125

126 **2. Materials and methods**

127 **2.1 The CS07, SAPRC-11 and SAPRC-18 mechanisms**

128 Three different chemical mechanisms from the SAPRC mechanism family were used in this
129 study, i.e., the condensed SAPRC-07 (CS07) (Carter, 2010), the standard SAPRC-11 (S11)
130 (Carter and Heo, 2013), and the standard SAPRC-18 (S18) (Carter, 2020). These mechanisms
131 were selected to represent different levels of detail in gas-phase reactions in a regional chemical
132 transport model. The CS07 was derived from the widely used SAPRC-07 mechanism and has
133 a high condensation level similar to that of the Carbon Bond mechanism, which is also widely
134 used. The S11 is an updated version of the SAPRC-07 mechanism, with significant revisions
135 made to the aromatic chemistry. The S11 mechanism employed in this study is identical to that
136 utilized in our previous study (Kang et al., 2021). For a detailed description of CS07 and S11
137 regarding O_3 source apportionment and emission sensitivity, please refer to Kang et al. (2022).
138 The S18 mechanism represents a complete update of the SAPRC mechanism since SAPRC-07.
139 S18 incorporates a greater number of model species, a more explicit representation of peroxy



radical chemistry, and a lumping scheme that is more suitable for predicting secondary organic aerosol (SOA) formation. Due to these modifications, S18 is more extensive than S11 in terms of both the number of species and chemical reactions. Although it has been successfully applied in photochemical box models (Jiang et al., 2020; Li et al., 2022a, b), it has not yet been implemented in 3D regional CTMs.

2.2. Anthropogenic emission inventories

The present study compares two widely used anthropogenic emission inventories, MEIC (<http://www.meicmodel.org>) and REAS 3.1 (<https://www.nies.go.jp/REAS/>), to investigate O₃ pollution in China. The emission data from these inventories were processed using an in-house emission processor. Detailed VOC speciation profiles selected from the US EPA-developed SPECIATE database were processed using the speciation profile processor from W.P.L. Carter (2015) to generate profiles for the CS07, SAPRC-11, and SAPRC-18 mechanisms, which are used to estimate emissions of CMAQ-ready VOCs. The MEIC emission inventory includes only emission estimates in China, whereas the REAS emission inventory has complete spatial coverage for Asian countries. In the MEIC simulation, emissions from other countries are supplemented using data from the REAS inventory.

2.3 Model application

The CS07, S11, and S18 mechanisms were incorporated into the CMAQ model (version 5.0.2) to evaluate the differences of mechanisms and inventories in predicting O₃-8h, OH and NO₃ radicals, secondary inorganic aerosols, and reactive VOC species (HCHO) in July 2017 in China. The model domain, which covers China and surrounding areas in eastern and southeastern Asia at a 36 km × 36 km horizontal resolution, along with the locations of cities mentioned in the manuscript, is illustrated in Figure S1.

The simulations included model runs with the following combinations: S11 mechanism with MEIC inventory (S11-MEIC), S11 with REAS (S11-REAS), CS07 with MEIC (CS07-MEIC), CS07 with REAS (CS07-REAS), and S18 with REAS (S18-REAS). It should be noted that while the MEIC emission inventory is for 2017, the most recent year in the REAS inventory is 2015, which is the one used in the current study. As the MEIC emission inventory encompasses only emissions from China, emissions from other regions were based on REAS, even when the simulations were mentioned using the MEIC inventory.



172 The July anthropogenic emission inventories from MEIC and REAS were processed using
173 an in-house emission processor, with updated speciation profiles employed to generate CMAQ-
174 ready VOC emissions (Kang et al., 2022). The speciation profiles for different chemical
175 mechanisms were derived from the same detailed speciation profiles extracted from the
176 SPECIATE database. Comprehensive overviews of MEIC and REAS inventories were
177 provided by Kang et al. (2022). Comparisons of major species, including NO_x (NO+NO₂), SO₂,
178 ethene (ETHENE), formaldehyde (HCHO), higher olefins (OLE) (comprising OLE1 and
179 OLE2, which are lumped alkene species with propylene and trans-2-pentene as representative
180 compounds), isoprene (ISOPRENE), and monoterpenes (TRP1), are shown in [Tables S1-S2](#)
181 [and Figures S2-S3](#) for municipalities and provinces in July 2017. Note that OLE and TRP1
182 emissions are for the S11 mechanisms. Emissions for CS07 are similar but some of the species
183 in OLE and TRP1 are explicit species in S18. There are notable spatial differences in the
184 weekday emissions of HCHO, ETHENE, OLE, SO₂, and NO_x between MEIC and REAS.
185 Specifically, REAS exhibits higher HCHO emissions in locations like Beijing, Tianjin, Henan,
186 Shanghai, and Guangzhou than MEIC ([Figure S2](#)). In the south of Henan, ethene emissions are
187 significantly higher in REAS relative to MEIC. The emissions of OLE in REAS are lower than
188 those in MEIC in Beijing, Tianjin, Shanghai, Guangzhou, Chengdu, and Chongqing. SO₂
189 emissions in MEIC are generally lower than those in REAS, except for Shanghai and
190 Guangzhou. NO_x emissions differ significantly between MEIC and REAS. In eastern China,
191 including cities like Shanghai and Guangzhou, NO_x emissions from REAS are typically lower
192 than those from MEIC, although some areas demonstrate a notable increase. These
193 discrepancies inevitably affect the accuracy of air pollutant predictions, underscoring the
194 necessity for a comprehensive assessment of emission inventories in the development of
195 effective pollution control policies.

196 Biogenic emissions were generated using the Model of Emissions of Gases and Aerosols
197 from Nature (MEGAN) version 2.10, which has been observed to emit higher levels of isoprene
198 and monoterpenes in comparison to anthropogenic sources ([Figure S3](#)). Open burning
199 emissions were produced using FINN inventory from the National Center for Atmospheric
200 Research (NCAR) (Wiedinmyer et al., 2011). Sea salt and windblown dust emissions were
201 simulated online using the CMAQ model. Initial and boundary conditions for the model
202 simulation were generated using CMAQ default profiles. The initial three days of the
203 simulation serve as a spin-up and are excluded from subsequent analyses.

204 Meteorological inputs were generated using the Weather Research and Forecasting (WRF)
205 model version 4.2 for the 36×36 km domain with 44 vertical layers. The initial and boundary



206 conditions for WRF were derived from the global reanalysis data FNL (available at
207 <https://rda.ucar.edu/datasets/ds083.2/>). Further details on the configuration of WRF model can
208 be found in the work of Kang et al. (2022). WRF-derived meteorological parameters, including
209 temperature and relative humidity at a height of 2 m above the surface and wind speed and
210 direction at 10 m, have been validated against observational data from the National Climatic
211 Data Center (NCDC), demonstrating good performance (Kang et al., 2021).

212

213 **2.4 Sensitivity of O₃ and related pollutants to emission controls across different** 214 **mechanisms and inventories**

215 A large number of sensitivity simulations with systematic reductions in NO_x and VOC
216 emissions were conducted to explore variations in the sensitivity of O₃-8h and related
217 pollutants to emission reductions across different mechanisms and inventories. Three sets of
218 simulations were performed for each mechanism/inventory combination considered in this
219 study (see section 2.3). In the first set of simulations, NO_x emissions were reduced by 20, 40,
220 50, 60, and 80%, while the emissions of VOCs were maintained at their base-case level. In the
221 second set of simulations, VOC emissions were reduced by 20, 40, 50, 60, and 80%, while NO_x
222 emissions remained constant. In the third set of simulations, both NO_x and VOC emissions
223 were reduced by 20-80%.

224

225 **3. Results and discussion**

226 **3.1 Model evaluation of O₃ and PM_{2.5} predictions across various mechanisms and** 227 **inventories**

228 Observations of O₃-8h and PM_{2.5} at a large number of surface monitoring stations nationwide
229 in July 2017 were obtained from the publication website of the China National Environmental
230 Monitoring Center (<http://www.cnemc.cn>). The model performance statistics were evaluated
231 separately for different regions: the North China Plain (NCP), Yangtze River Delta (YRD),
232 Central China (Center), Pearl River Delta (PRD), and Sichuan Basin (SCB). Specifically, NCP
233 includes Beijing, Tianjin, and some cities in Hebei and Shandong provinces; Center includes
234 cities in the provinces of Henan, Hubei, Hunan, and Jiangxi; YRD includes Shanghai and some
235 cities in the provinces of Anhui, Jiangsu, and Zhejiang; PRD includes Shenzhen and some
236 cities in Guangdong province; and SCB includes Chongqing and some cities in Sichuan
237 province. As shown in [Figures S4-S5](#), the model performance for O₃-8h and PM_{2.5} predicted
238 by different mechanisms and emission inventories in major regions of China exhibits large
239 variations, due to differences in climate, topography, and emission sources. Overall, the



average values of mean normalized bias (MNB) and mean normalized error (MNE) for O₃-8h predictions across all combinations of mechanisms and inventories are generally within the model performance criteria suggested by the US EPA in most regions, except for underprediction in the PRD. Similarly, the model shows good performance for PM_{2.5} in most areas, except for the PRD region, where the mean fractional biases (MFB) for PM_{2.5} using S18-REAS, CS07-REAS, and S11-REAS are slightly outside the recommended range (Boylan and Russell, 2006). The underestimation of PM_{2.5} predictions using REAS in the PRD is likely related to biases in this inventory specific to this region.

3.2 Spatial variations in predictions of O₃ and related pollutants by different mechanisms and inventories

Figure 1 shows the spatial distribution of monthly averaged O₃-8h concentrations predicted by S11-MEIC during summer, along with the absolute differences between O₃-8h predictions from S11-MEIC and those from other mechanisms and inventories. Based on S11-MEIC, high O₃-8h levels exceeding 80 ppb occurred in eastern China, especially in Beijing, Tianjin, Hebei, northern Henan, SCB, and Shanghai. Extremely high O₃-8h levels above 100 ppb are also observed over the Bohai Bay and the Yellow Sea, likely due to regional transport of polluted air from the continent, reduced NO_x titration with O₃, and lower O₃ dry deposition velocities over the ocean. Similar spatial distributions of O₃-8h concentrations are also found in the simulations using other mechanisms and inventories (Figure S6). In comparison, O₃-8h concentrations predicted by S11-REAS are generally 2–7 ppb higher than those by S11-MEIC in most parts of China, especially in the central region, Zhejiang, and Fujian provinces, but about 2–7 ppb lower in Beijing, Shanghai, Chengdu, and the PRD region. S18-REAS predicted significantly lower O₃-8h levels, with reductions greater than 7 ppb in regions such as Beijing, Tianjin, Hebei, Shanghai, SCB, PRD, and other developed areas such as Zhengzhou and Hefei. In contrast, CS07-MEIC predicted lower O₃-8h levels overall, with apparent reductions of ~6–7 ppb in the SCB, central China, and coastal areas near Shanghai. Similarly, CS07-REAS also showed generally lower O₃-8h concentrations compared to S11-MEIC, particularly in Chengdu, Luoyang, Shanghai, Guangzhou, Ningbo, Hefei, Nanchang, and the Yellow Sea (~7 ppb lower or more), although some locations exhibit higher O₃-8h levels than those predicted by S11-MEIC. These discrepancies highlight that the accuracy of O₃ predictions is sensitive to variations in photochemical mechanisms and emission inventories. This underscores the importance of adopting and comparing multiple mechanisms and inventories when developing region-specific pollution control policies.



274 [Figure 2](#) illustrates the differences in spatial distribution of monthly averaged SIA
275 concentrations modeled with different mechanisms and inventories. According to S11-MEIC,
276 high SIA concentrations are mainly concentrated in NCP and SCB, exceeding $15 \mu\text{g m}^{-3}$. High
277 SIA concentrations are also found in Bohai Bay, likely due to long-range transport of polluted
278 air from land sources. Compared to S11-MEIC, S11-REAS predicts higher SIA concentrations
279 in most regions, with increases of $> 1 \mu\text{g m}^{-3}$ in most areas, especially in NCP, Henan, and
280 SCB (higher by about $6 \mu\text{g m}^{-3}$ or even more). Nationwide, SIA concentrations predicted by
281 S18-REAS are generally higher than those predicted by S11-MEIC, with increases of up to 6
282 $\mu\text{g m}^{-3}$ or more in the NCP, Central China, SCB, Bohai Bay, and the Yellow Sea. CS07-MEIC
283 shows similar SIA levels to S11-MEIC, with slightly lower concentrations of $\sim 1 \mu\text{g m}^{-3}$ in SCB
284 and Bohai Bay. The spatial differences in SIA predictions between CS07-REAS and S11-
285 MEIC are similar to those between S11-REAS and S11-MEIC, suggesting that SIA
286 concentrations from CS07-REAS and S11-REAS are comparable.

287

288 **3.3 Impacts of mechanisms and inventories on predicted atmospheric oxidation capacity**

289 Atmospheric oxidation capacity (AOC), which governs the removal rate of primary pollutants
290 and the production of secondary pollutants (Elshorbany et al., 2009; Prinn, 2003), is primarily
291 controlled by the hydroxyl (OH) and nitrate (NO_3) radicals in the atmosphere (Geyer et al.,
292 2001; Liu et al., 2022). The spatial differences in OH and NO_3 predictions for different
293 mechanisms and inventories are illustrated in [Figures 3-4](#).

294 S11-MEIC predicts high OH concentrations exceeding $3.7 \times 10^6 \text{ molecules cm}^{-3}$ (0.15 ppt)
295 mainly in northern China, including NCP, Inner Mongolia, and some western sites. Compared
296 to S11-MEIC, S11-REAS predicts lower OH concentrations in NCP, Jiangsu, Shanghai, PRD,
297 SCB, and other urban nuclei but higher concentrations in rural areas. In contrast, S18-REAS
298 predicts higher OH concentrations than S11-MEIC in most regions, except in some northern
299 locations. CS07-MEIC produces elevated OH concentrations in northwestern China, Chengdu,
300 Chongqing, Shanghai, Hebei, Shandong, and northern Henan, but lower OH levels in other
301 regions. Similar to S11-REAS, CS07-REAS shows much higher OH levels in northwestern
302 China but lower OH levels in eastern regions than S11-MEIC. The variability in OH levels can
303 significantly affect the formation of O_3 and other gaseous and particulate pollutants.

304 The spatial distribution of NO_3 concentrations modeled by S11-MEIC exhibits high values
305 in Xinjiang, Inner Mongolia, NCP, and Bohai Bay, with NO_3 concentrations reaching up to 20
306 ppt. Obvious differences in NO_3 predictions between S11-REAS and S11-MEIC are primarily



307 observed in Xinjiang and Inner Mongolia, with smaller differences in other regions. S18-REAS
308 generally predicted higher NO₃ concentrations than S11-MEIC, especially in Xinjiang, Inner
309 Mongolia, Bohai Bay, Yellow Sea, and Taiwan Strait, by ~6 ppt or more. In contrast, CS07-
310 MEIC consistently predicts lower NO₃ levels than S11-MEIC. CS07-REAS predicted lower
311 NO₃ concentrations in the eastern regions but higher concentrations in parts of Xinjiang
312 compared to S11-MEIC.

313

314 **3.4 Impacts of mechanisms and inventories on HCHO prediction**

315 Spatial variations in AOC, as reflected in OH and NO₃ predictions from different mechanisms
316 and inventories, imply that photochemical formation and loss rates for air toxics may also vary
317 depending on the mechanism and inventory used. To explore how these variations affect the
318 modeling results for gaseous pollutants, we examined HCHO, one of the most important
319 gaseous air toxics with both primary and secondary sources. It is also a significant contributor
320 to O₃ formation and OH production, thus playing a crucial role in tropospheric photochemistry
321 (Wang et al., 2017; Zhang et al., 2013).

322 HCHO concentrations predicted by S11-MEIC are generally high in the SCB and eastern
323 China, areas with significant biogenic VOC emissions (Kang et al., 2023), particularly in
324 Chengdu, Shanghai, and Changsha, where HCHO concentrations reach or exceed 7 ppb (Figure
325 5). This suggests that a significant fraction of the HCHO is due to secondary formation. HCHO
326 levels predicted by S11-REAS are similar to those predicted by S11-MEIC, with only minor
327 differences of less than 1 ppb. In contrast, S18-REAS predicts significantly lower HCHO levels
328 than S11-MEIC, with differences > 1 ppb, especially in SCB, NCP, PRD, YRD, and central
329 China. CS07-MEIC and CS07-REAS predict higher HCHO levels than S11-MEIC, especially
330 in SCB and eastern China, with differences exceeding 1 ppb. These results indicate that HCHO
331 predictions are more strongly influenced by photochemical mechanisms than by uncertainties
332 in emission inventories, due to its secondary formation.

333

334 **3.5 Impacts of mechanisms and inventories on the sensitivity of O₃ and related pollutants 335 to emission controls**

336 Figures 6-10 and S6-S15 display the fractional changes in predictions of O₃ and related
337 pollutants due to NO_x and VOC reductions using various mechanisms and inventories.

338 **3.5.1 Impacts of mechanisms and inventories on O₃ sensitivity to emission controls**

339 For all mechanisms and inventories, O₃-8h concentrations consistently decrease with
340 reductions in NO_x, VOCs, or both in all five cities during summer. The efficiency of emission



controls improves with increasingly higher emission reductions of NO_x , VOCs. These trends are consistent with the findings of Kang et al. (2021), suggesting that the mechanisms and inventories do not affect the trend of change in O_3 , but do affect the magnitude of the change. These results also show that during summer, the sensitivity of O_3 formation to NO_x and VOCs is in transition or NO_x -limited regimes. In Beijing, when NO_x emissions are reduced, CS07-MEIC and CS07-REAS show the largest O_3 -8h reductions compared to other mechanisms and inventories, while S18-REAS exhibits the smallest changes, especially with larger NO_x reductions. In Shanghai, the largest O_3 -8h reductions due to NO_x controls are observed with CS07-REAS, followed by S11-REAS, while S18-REAS again shows the smallest changes. In Changsha, there are no significant differences among mechanisms and inventories in the sensitivity tests. In Shenzhen, S11-REAS shows the greatest decreases in O_3 -8h, followed by CS07-REAS and S18-REAS, while S11-MEIC and CS07-MEIC show the smallest changes. Except for S18-REAS, predictions from other mechanisms and inventories are similar in Chongqing.

When only VOC emissions are reduced in Beijing, S11-MEIC predicts the largest O_3 -8h reductions, while CS07-REAS predicts the smallest changes. Similar patterns are found in Shanghai and Changsha, with larger differences among different mechanisms and inventories in Shanghai. In Shenzhen, S11-MEIC also exhibits the largest O_3 -8h decreases, followed by CS07-MEIC, while CS07-REAS, S11-REAS, and S18-REAS show smaller changes. In Chongqing, S18-REAS predicts the largest changes and CS07-MEIC the smallest, although the differences among these scenarios are not substantial. When both NO_x and VOC emissions are reduced, the predicted change rates of O_3 -8h do not vary much across different mechanisms and emission inventories for all five cities. Additionally, the sensitivity tests for Shenzhen, as presented in Figure 6, suggest that differences in emission inventories may have a greater impact on emission control outcomes than differences in chemical mechanisms.

Figure S6 illustrates the national-scale relative changes in O_3 -8h due to NO_x emission reductions evaluated using different mechanisms and inventories. The results are consistent with those shown in Figure 6, with the greatest O_3 -8h reductions occurring in the SCB, Central, and YRD. For all mechanisms and inventories, increasingly higher NO_x reductions generally lead to increasingly lower O_3 in summer, with relative changes in O_3 -8h ranging from approximately 5% to 60% as NO_x reductions increase from 20% to 80%. In comparison, the O_3 -8h reductions predicted by S18-REAS are less pronounced than other mechanisms and inventories in most areas. Similar to NO_x reductions, higher VOC reductions typically result in larger O_3 reductions in summer, with significant reductions observed in NCP, Chengdu,



PRD, Shanghai, and Bohai Bay. The relative changes in O_3 -8h increase from 5% to 40% as VOC reductions increase from 20% to 80% in these areas (Figure S7). The comparison between Figure S6 and Figure S7 suggests that NO_x reduction tends to be more effective in controlling O_3 pollution in non-VOC-limited regions than VOC reduction, given the same level of emission reduction.

380

3.5.2 Impacts of mechanisms and inventories on SIA sensitivity to emission controls

Reducing NO_x emissions typically leads to decreasing SIA levels across the five cities, with the efficiency of reductions improving as NO_x reduction increases. As illustrated in Figure 7, the predicted changes in SIA are quite similar for different mechanisms and inventories. However, VOC controls do not always effectively reduce SIA concentrations, likely attributable to an increase in NO_3 radicals, as shown in Figure 9. In Beijing, changes in SIA in response to VOC reductions vary with mechanisms and inventories. For S11-MEIC and CS07-MEIC, SIA concentration first increases and then decreases with decreasing VOCs. S18-REAS shows a general decrease in SIA concentrations with decreasing VOCs. In contrast, CS07-REAS and S11-REAS predict an increase in SIA concentrations with VOC reductions, with the rate of SIA growth initially increasing and then decreasing as VOC emission decreases. In Shanghai, VOC reductions generally increase SIA concentrations across all mechanisms and inventories, especially for CS07-REAS and S11-REAS, which show that SIA concentrations consistently increase as VOCs are progressively reduced. In Changsha, SIA concentrations also consistently increase with increasing VOC reductions for all mechanisms and inventories. In Shenzhen, SIA concentrations increase with VOC reductions; however, the changes are more pronounced for S11-REAS compared to the less significant variations observed for CS07-MEIC. Except for S18-REAS, Chongqing shows an increase in SIA concentrations with VOC reductions, particularly for CS07-REAS. Overall, simultaneous reductions in NO_x and VOCs decrease SIA levels in most cities, similar to the effects of NO_x controls alone.

Figure S8 shows the relative changes in SIA due to NO_x controls on a national scale, using different mechanisms and inventories. The stepwise reductions in NO_x emissions lead to an overall decrease in SIA concentrations, with the most pronounced reductions observed in the NCP, SCB, Jiangsu, Bohai Bay, and Yellow Sea. The decreases in SIA increase from ~5% to 60% as NO_x reduction increases from 20% to 80%. On the contrary, VOC reduction causes an overall increase in SIA concentrations (Figure S9), indicating that VOC controls are less effective than NO_x controls in reducing SIA levels during summer. Notably, the largest increases in SIA are seen in SCB, Central, and YRD, where SIA increases grow from ~ 6% to



409 30% as VOC reduction increases from 20% to 80%. In comparison, S18-REAS shows
410 relatively smaller changes in SIA, with some areas in NCP showing obvious decreases in SIA
411 concentrations.

412

413 **3.5.3 Impacts of mechanisms and inventories on OH and NO₃ sensitivity**

414 As shown in [Figures 8-9](#), the effects of NO_x reductions on OH concentrations vary depending
415 on the mechanism and inventory used. In most regions, OH production decreases with reducing
416 NO_x emissions, likely due to the decrease in O₃ concentrations, as O₃ photolysis in the presence
417 of water vapor is a significant source of atmospheric OH (Seinfeld and Pandis, 2016). Except
418 for Shenzhen, CS07-MEIC and CS07-REAS predict the largest decreases in OH due to NO_x
419 control in other cities, while S18-REAS predicts the smallest OH change rates. In Shenzhen,
420 OH levels predicted by S11-MEIC and CS07-MEIC initially increase and then decrease as NO_x
421 emissions decrease, while those predicted by S18-REAS, CS07-REAS, and S11-REAS exhibit
422 a consistent decrease in OH levels. When only VOCs are reduced, the changes in OH vary
423 across different mechanisms and inventories. In Beijing, except for S18-REAS, OH
424 concentration initially increases and then decreases with decreasing VOC emissions. In
425 Shanghai, OH concentrations from CS07-REAS and S11-REAS basically increase with
426 decreasing VOCs, while those from CS07-MEIC and S11-MEIC show an initial increase
427 followed by a decrease. S18-REAS predicts a general decrease of OH with decreasing VOCs
428 in Beijing and Shanghai. In Changsha, OH concentrations consistently increase with reduced
429 VOCs across all mechanisms and inventories, with CS07-REAS showing a rapid increase of
430 up to 75%. In Shenzhen, OH levels from CS07-REAS, S11-REAS, and S18-REAS increase
431 with decreasing VOCs, while those from S11-MEIC and CS07-MEIC decrease. In Chongqing,
432 all mechanisms and inventories except S18-REAS predict an increase in OH concentrations
433 with decreasing VOCs, with CS07-MEIC showing a significant increase of up to 75%. When
434 both NO_x and VOC emissions are reduced, OH concentrations generally increase for all
435 mechanisms and inventories, although the relative changes are relatively small (< 25%).

436 [Figures S10-S11](#) display the spatial distribution of OH changes due to incremental emission
437 controls across different mechanisms and inventories. There is a nationwide decrease in OH
438 concentrations due to NO_x reductions, with more pronounced decreases in central and eastern
439 China, where OH levels drop by ~ 20% to 80% as NO_x reduction increases from 20% to 80%.
440 Instead, VOC reductions generally lead to increased OH concentrations across most of China,
441 significantly in some regions with large vegetation cover (Kang et al., 2023), such as central
442 and southeastern China. In these areas, OH levels increase by 20~200% in response to stepwise



VOC reductions. This increase occurs because high atmospheric VOC concentrations in rural and vegetation-rich areas react with OH radicals to produce RO₂ and HO₂, depleting OH, thus reducing VOCs in these areas increases OH levels. However, in some urban centers, such as Beijing and Shanghai, changes in OH levels due to VOC controls depend on the extent of reduction and the choice of mechanism and inventory.

Similar to OH, NO₃ levels predicted by different mechanisms and inventories basically decrease with decreasing NO_x emissions, likely related to the decline of O₃ concentrations since NO₃ radicals are predominantly formed by the reaction of NO₂ with O₃ (Geyer et al., 2001). In general, the change rates of NO₃ due to NO_x reductions are higher for CS07-MEIC and CS07-REAS, while lower for S18-REAS. When VOC emissions are reduced, NO₃ production increases, except for S18-REAS. In Changsha, a particularly dramatic increase of over 200% and 150% is observed for CS07-REAS and CS07-MEIC, respectively, when VOC emissions are cut by 80%. This increase in NO₃ radicals could be attributed to a decline in the rapid reaction of NO₃ with unsaturated hydrocarbons. However, for S18-REAS, NO₃ concentrations decrease with decreasing VOCs in Beijing, Shanghai, and Chongqing. Unlike OH, simultaneous reductions in NO_x and VOCs result in lower NO₃ levels across all mechanisms and inventories.

Figures S12-13 illustrate the spatial variation in NO₃ changes due to systematic emission reductions for all mechanisms and inventories. NO₃ radicals show a decreasing trend, particularly in eastern China, where reductions in NO₃ levels vary from 40% to 100%. Except for S18-REAS, other mechanisms and inventories generally predict a nationwide increase in NO₃ radicals with reduced VOCs, particularly in central and southeastern China, where NO₃ levels increase by ~ 30 – 300% or even more with increasing VOC reductions. S18-REAS predicts a decrease in NO₃ levels with reduced VOCs in some megacities such as Beijing, Shanghai, Chengdu, and Chongqing, while NO₃ levels increase elsewhere.

3.5.4 Impacts of mechanisms and inventories on the sensitivity of secondary gaseous pollutants to emission controls

As shown in Figure 10, HCHO concentrations decrease with decreasing NO_x emissions, likely due to decreased AOC, as evidenced by decreased OH and NO₃ levels. This indicates that secondary formation from the oxidation of atmospheric VOCs is the dominant source of HCHO, in accordance with previous studies (Wang et al., 2017; Yang et al., 2019; Zhang et al., 2013). In addition, the most significant decreases in HCHO levels due to NO_x reductions are observed for CS07-REAS in all five cities, particularly in Changsha and Chongqing, where HCHO levels



drop by about 40%. When VOCs are reduced alone, HCHO levels decrease linearly across all mechanisms and inventories, a trend similar to the simultaneous reduction of NO_x and VOCs. Variations in HCHO changes across different mechanisms and inventories suggest the need to evaluate different mechanisms and inventories when formulating regional emission control policies for carbonyl pollution.

Figures S14- S15 illustrate the spatial distribution of relative changes in HCHO due to NO_x and VOC controls using different mechanisms and inventories. VOC and NO_x controls lead to reductions in HCHO concentration, especially in eastern China. However, VOC controls generally leads to larger reductions in HCHO concentrations (~10–80%) than NO_x controls (~4 – 40%), as shown in Figures S14-15 and 10. This suggests that VOC controls are also essential and more effective for reducing secondary gaseous organic pollutants in the atmosphere.

4. Conclusions

This study utilized the CMAQ model to evaluate the impacts of different mechanisms and inventories on the prediction of O₃ and other air pollutants. It also examined how these mechanisms and inventories affect the sensitivity of O₃ and related species to emission reductions. For maximum daily average 8-hour O₃ (O₃-8h), relative reductions predicted using different emission inventory and mechanism combinations are consistent for up to 80% NO_x or VOC reductions, with maximum differences of approximately 15%. For secondary inorganic aerosols (SIA), while the predicted relative changes in their daily average concentrations due to NO_x reductions are quite similar, very large differences of up to 30% occur for VOC reductions. Sometimes even the direction of change (i.e., increase or decrease) is different. For the oxidants OH and NO₃ radicals, the uncertainties in the relative changes due to emission changes are even larger among different inventory-mechanism combinations, sometimes by as much as 200%. Our results suggest that while the O₃-8h responses to emission changes are not sensitive to the choice of chemical mechanism and emission inventories, using a single model and mechanism to evaluate the effectiveness of emission controls on SIA and atmospheric oxidation capacity may have large errors. For these species, the evaluation of the control strategies may require an ensemble approach with multiple inventories and mechanisms.

Data availability. The dataset for this paper is available upon request from the corresponding author (qying@ust.hk).



510 **Author contributions.** QY designed the study. QY and MJK developed the CMAQ model.
511 MJK conducted the simulations, analyzed the data, and wrote the manuscript. All coauthors
512 contributed to the discussion and revision of the paper.

513 **Competing interests.** The authors declare that they have no conflict of interest.

514 **Acknowledgments**

515 This work was partly supported by the National Natural Science Foundation of China (No.
516 42307142).



References

- Akimoto, H., Ohara, T., Kurokawa, J., and Horii, N.: Verification of energy consumption in China during 1996–2003 by using satellite observational data, *Atmospheric Environment*, 40, 7663–7667, <https://doi.org/10.1016/j.atmosenv.2006.07.052>, 2006.
- Boylan, J. W. and Russell, A. G.: PM and light extinction model performance metrics, goals, and criteria for three-dimensional air quality models, *Atmospheric Environment*, 40, 4946–4959, <https://doi.org/10.1016/j.atmosenv.2005.09.087>, 2006.
- Bray, C. D., Strum, M., Simon, H., Riddick, L., Kosusko, M., Menetrez, M., Hays, M. D., and Rao, V.: An assessment of important SPECIATE profiles in the EPA emissions modeling platform and current data gaps, *Atmospheric Environment*, 207, 93–104, <https://doi.org/10.1016/j.atmosenv.2019.03.013>, 2019.
- Byun, D. and Schere, K. L.: Review of the Governing Equations, Computational Algorithms, and Other Components of the Models-3 Community Multiscale Air Quality (CMAQ) Modeling System, *Applied Mechanics Reviews*, 59, 51–77, <https://doi.org/10.1115/1.2128636>, 2006.
- Carter, W. P. L.: Development of a condensed SAPRC-07 chemical mechanism, *Atmospheric Environment*, 44, 5336–5345, <https://doi.org/10.1016/j.atmosenv.2010.01.024>, 2010.
- Carter, W. P. L.: Development of a database for chemical mechanism assignments for volatile organic emissions, *Journal of the Air & Waste Management Association*, 65, 1171–1184, <https://doi.org/10.1080/10962247.2015.1013646>, 2015.
- Carter, W. P. L.: Documentation of the SAPRC-18 mechanism, Report to the California Air Resources Board, 2020.
- Carter, W. P. L. and Heo, G.: Development of revised SAPRC aromatics mechanisms, *Atmos. Environ.*, 77, 404–414, <https://doi.org/10.1016/j.atmosenv.2013.05.021>, 2013.
- Du, H., Yan, M., Liu, X., Zhong, Y., Ban, J., Lu, K., and Li, T.: Exposure to Concurrent Heatwaves and Ozone Pollution and Associations with Mortality Risk: A Nationwide Study in China, *Environmental Health Perspectives*, 132, 047012, <https://doi.org/10.1289/EHP13790>, 2024.
- Elshorbany, Y. F., Kurtenbach, R., Wiesen, P., Lissi, E., Rubio, M., Villena, G., Gramsch, E., Rickard, A. R., Pilling, M. J., and Kleffmann, J.: Oxidation capacity of the city air of Santiago, Chile, *Atmospheric Chemistry and Physics*, 9, 2257–2273, <https://doi.org/10.5194/acp-9-2257-2009>, 2009.
- Feng, Z., Xu, Y., Kobayashi, K., Dai, L., Zhang, T., Agathokleous, E., Calatayud, V., Paoletti, E., Mukherjee, A., Agrawal, M., Park, R. J., Oak, Y. J., and Yue, X.: Ozone pollution threatens the production of major staple crops in East Asia, *Nat Food*, 3, 47–56, <https://doi.org/10.1038/s43016-021-00422-6>, 2022.
- Finlayson-Pitts, B. J. and Pitts Jr, J. N.: *Chemistry of the upper and lower atmosphere: theory, experiments, and applications*, Elsevier, 1999.
- Geyer, A., Alicke, B., Konrad, S., Schmitz, T., Stutz, J., and Platt, U.: Chemistry and oxidation capacity of the nitrate radical in the continental boundary layer near Berlin, *Journal of Geophysical Research: Atmospheres*, 106, 8013–8025, <https://doi.org/10.1029/2000JD900681>, 2001.
- Ghude, S. D., Chate, D. M., Jena, C., Beig, G., Kumar, R., Barth, M. C., Pfister, G. G., Fadnavis, S., and Pithani, P.: Premature mortality in India due to PM_{2.5} and ozone exposure, *Geophysical Research Letters*, 43, 4650–4658, <https://doi.org/10.1002/2016GL068949>, 2016.
- Griffith, S. M., Hansen, R. F., Dusanter, S., Michoud, V., Gilman, J. B., Kuster, W. C., Veres, P. R., Graus, M., de Gouw, J. A., Roberts, J., Young, C., Washenfelder, R., Brown, S. S., Thalman, R., Waxman, E., Volkamer, R., Tsai, C., Stutz, J., Flynn, J. H., Grossberg,



- 567 N., Lefer, B., Alvarez, S. L., Rappenglueck, B., Mielke, L. H., Osthoff, H. D., and
568 Stevens, P. S.: Measurements of hydroxyl and hydroperoxy radicals during CalNex-
569 LA: Model comparisons and radical budgets, *Journal of Geophysical Research:*
570 *Atmospheres*, 121, 4211–4232, <https://doi.org/10.1002/2015JD024358>, 2016.
- 571 Hu, J., Li, X., Huang, L., Ying, Q., Zhang, Q., Zhao, B., Wang, S., and Zhang, H.: Ensemble
572 prediction of air quality using the WRF/CMAQ model system for health effect studies
573 in China, *Atmospheric Chemistry and Physics*, 17, 13103–13118,
574 <https://doi.org/10.5194/acp-17-13103-2017>, 2017a.
- 575 Hu, J., Huang, L., Chen, M., Liao, H., Zhang, H., Wang, S., Zhang, Q., and Ying, Q.: Premature
576 Mortality Attributable to Particulate Matter in China: Source Contributions and
577 Responses to Reductions, *Environ. Sci. Technol.*, 51, 9950–9959,
578 <https://doi.org/10.1021/acs.est.7b03193>, 2017b.
- 579 Jiang, J., Carter, W. P. L., Cocker, D. R. I., and Barsanti, K. C.: Development and Evaluation
580 of a Detailed Mechanism for Gas-Phase Atmospheric Reactions of Furans, *ACS Earth*
581 *Space Chem.*, 4, 1254–1268, <https://doi.org/10.1021/acsearthspacechem.0c00058>,
582 2020.
- 583 Kang, M., Zhang, J., Zhang, H., and Ying, Q.: On the Relevancy of Observed Ozone Increase
584 during COVID-19 Lockdown to Summertime Ozone and PM_{2.5} Control Policies in
585 China, *Environ. Sci. Technol. Lett.*, 8, 289–294,
586 <https://doi.org/10.1021/acs.estlett.1c00036>, 2021.
- 587 Kang, M., Hu, J., Zhang, H., and Ying, Q.: Evaluation of a highly condensed SAPRC chemical
588 mechanism and two emission inventories for ozone source apportionment and emission
589 control strategy assessments in China, *Science of The Total Environment*, 813, 151922,
590 <https://doi.org/10.1016/j.scitotenv.2021.151922>, 2022.
- 591 Kang, M., Zhang, H., and Ying, Q.: Enhanced summertime background ozone by
592 anthropogenic emissions – Implications on ozone control policy and health risk
593 assessment, *Atmospheric Environment*, 314, 120116,
594 <https://doi.org/10.1016/j.atmosenv.2023.120116>, 2023.
- 595 Kim, Y., Sartelet, K., and Seigneur, C.: Comparison of two gas-phase chemical kinetic
596 mechanisms of ozone formation over Europe, *J Atmos Chem*, 62, 89–119,
597 <https://doi.org/10.1007/s10874-009-9142-5>, 2009.
- 598 Lei, Y., Zhang, Q., He, K. B., and Streets, D. G.: Primary anthropogenic aerosol emission
599 trends for China, 1990–2005, *Atmospheric Chemistry and Physics*, 11, 931–954,
600 <https://doi.org/10.5194/acp-11-931-2011>, 2011.
- 601 Li, J., Zhang, H., and Ying, Q.: Comparison of the SAPRC07 and SAPRC99 photochemical
602 mechanisms during a high ozone episode in Texas: Differences in concentrations, OH
603 budget and relative response factors, *Atmospheric Environment*, 54, 25–35,
604 <https://doi.org/10.1016/j.atmosenv.2012.02.034>, 2012.
- 605 Li, K., Jacob, D. J., Liao, H., Shen, L., Zhang, Q., and Bates, K. H.: Anthropogenic drivers of
606 2013–2017 trends in summer surface ozone in China, *Proc Natl Acad Sci USA*, 116,
607 422–427, <https://doi.org/10.1073/pnas.1812168116>, 2019.
- 608 Li, K., Zhang, X., Zhao, B., Bloss, W. J., Lin, C., White, S., Yu, H., Chen, L., Geng, C., Yang,
609 W., Azzi, M., George, C., and Bai, Z.: Suppression of anthropogenic secondary organic
610 aerosol formation by isoprene, *npj Clim Atmos Sci*, 5, 1–9,
611 <https://doi.org/10.1038/s41612-022-00233-x>, 2022a.
- 612 Li, M., Zhang, Q., Streets, D. G., He, K. B., Cheng, Y. F., Emmons, L. K., Huo, H., Kang, S.
613 C., Lu, Z., Shao, M., Su, H., Yu, X., and Zhang, Y.: Mapping Asian anthropogenic
614 emissions of non-methane volatile organic compounds to multiple chemical
615 mechanisms, *Atmospheric Chemistry and Physics*, 14, 5617–5638,
616 <https://doi.org/10.5194/acp-14-5617-2014>, 2014.



- Li, N., He, Q., Greenberg, J., Guenther, A., Li, J., Cao, J., Wang, J., Liao, H., Wang, Q., and Zhang, Q.: Impacts of biogenic and anthropogenic emissions on summertime ozone formation in the Guanzhong Basin, China, *Atmospheric Chemistry and Physics*, 18, 7489–7507, <https://doi.org/10.5194/acp-18-7489-2018>, 2018.
- Li, Q., Jiang, J., Afreh, I. K., Barsanti, K. C., and Cocker III, D. R.: Secondary organic aerosol formation from camphene oxidation: measurements and modeling, *Atmospheric Chemistry and Physics*, 22, 3131–3147, <https://doi.org/10.5194/acp-22-3131-2022>, 2022b.
- Liu, T., Hong, Y., Li, M., Xu, L., Chen, J., Bian, Y., Yang, C., Dan, Y., Zhang, Y., Xue, L., Zhao, M., Huang, Z., and Wang, H.: Atmospheric oxidation capacity and ozone pollution mechanism in a coastal city of southeastern China: analysis of a typical photochemical episode by an observation-based model, *Atmospheric Chemistry and Physics*, 22, 2173–2190, <https://doi.org/10.5194/acp-22-2173-2022>, 2022.
- Lu, X., Hong, J., Zhang, L., Cooper, O. R., Schultz, M. G., Xu, X., Wang, T., Gao, M., Zhao, Y., and Zhang, Y.: Severe surface ozone pollution in China: A global perspective, *Environmental Science & Technology Letters*, 5, 487–494, 2018.
- Lu, X., Zhang, L., Wang, X., Gao, M., Li, K., Zhang, Y., Yue, X., and Zhang, Y.: Rapid Increases in Warm-Season Surface Ozone and Resulting Health Impact in China Since 2013, *Environ. Sci. Technol. Lett.*, 7, 240–247, <https://doi.org/10.1021/acs.estlett.0c00171>, 2020.
- Lyu, X., Li, K., Guo, H., Morawska, L., Zhou, B., Zeren, Y., Jiang, F., Chen, C., Goldstein, A. H., Xu, X., Wang, T., Lu, X., Zhu, T., Querol, X., Chatani, S., Latif, M. T., Schuch, D., Sinha, V., Kumar, P., Mullins, B., Seguel, R., Shao, M., Xue, L., Wang, N., Chen, J., Gao, J., Chai, F., Simpson, I., Sinha, B., and Blake, D. R.: A synergistic ozone-climate control to address emerging ozone pollution challenges, *One Earth*, 6, 964–977, <https://doi.org/10.1016/j.oneear.2023.07.004>, 2023.
- Ma, J. and van Aardenne, J. A.: Impact of different emission inventories on simulated tropospheric ozone over China: a regional chemical transport model evaluation, *Atmospheric Chemistry and Physics*, 4, 877–887, <https://doi.org/10.5194/acp-4-877-2004>, 2004.
- Placet, M., Mann, C. O., Gilbert, R. O., and Niefer, M. J.: Emissions of ozone precursors from stationary sources: a critical review, *Atmospheric Environment*, 34, 2183–2204, [https://doi.org/10.1016/S1352-2310\(99\)00464-1](https://doi.org/10.1016/S1352-2310(99)00464-1), 2000.
- Prinn, R. G.: The Cleansing Capacity of the Atmosphere, *Annual Review of Environment and Resources*, 28, 29–57, <https://doi.org/10.1146/annurev.energy.28.011503.163425>, 2003.
- Real, E., Megaritis, A., Colette, A., Valastro, G., and Messina, P.: Atlas of ozone chemical regimes in Europe, *Atmospheric Environment*, 320, 120323, <https://doi.org/10.1016/j.atmosenv.2023.120323>, 2024.
- Russell, A.: REGIONAL PHOTOCHEMICAL AIR QUALITY MODELING: Model Formulations, History, and State of the Science, *Annual Review of Environment and Resources*, 22, 537–588, <https://doi.org/10.1146/annurev.energy.22.1.537>, 1997.
- Saikawa, E., Kim, H., Zhong, M., Avramov, A., Zhao, Y., Janssens-Maenhout, G., Kurokawa, J., Klimont, Z., Wagner, F., Naik, V., Horowitz, L. W., and Zhang, Q.: Comparison of emissions inventories of anthropogenic air pollutants and greenhouse gases in China, *Atmospheric Chemistry and Physics*, 17, 6393–6421, <https://doi.org/10.5194/acp-17-6393-2017>, 2017.
- Seinfeld, J. H. and Pandis, S. N.: *Atmospheric Chemistry and Physics: From Air Pollution to Climate Change*, John Wiley & Sons, 1152 pp., 2016.



- 666 Sha, Q., Zhu, M., Huang, H., Wang, Y., Huang, Z., Zhang, X., Tang, M., Lu, M., Chen, C.,
667 Shi, B., Chen, Z., Wu, L., Zhong, Z., Li, C., Xu, Y., Yu, F., Jia, G., Liao, S., Cui, X.,
668 Liu, J., and Zheng, J.: A newly integrated dataset of volatile organic compounds (VOCs)
669 source profiles and implications for the future development of VOCs profiles in China,
670 *Science of The Total Environment*, 793, 148348,
671 <https://doi.org/10.1016/j.scitotenv.2021.148348>, 2021.
- 672 Streets, D. G., Bond, T. C., Carmichael, G. R., Fernandes, S. D., Fu, Q., He, D., Klimont, Z.,
673 Nelson, S. M., Tsai, N. Y., Wang, M. Q., Woo, J.-H., and Yarber, K. F.: An inventory
674 of gaseous and primary aerosol emissions in Asia in the year 2000, *Journal of*
675 *Geophysical Research: Atmospheres*, 108, <https://doi.org/10.1029/2002JD003093>,
676 2003.
- 677 Wang, C., Huang, X.-F., Han, Y., Zhu, B., and He, L.-Y.: Sources and Potential Photochemical
678 Roles of Formaldehyde in an Urban Atmosphere in South China, *Journal of*
679 *Geophysical Research: Atmospheres*, 122, 11,934–11,947,
680 <https://doi.org/10.1002/2017JD027266>, 2017.
- 681 West, J. J., Fiore, A. M., Horowitz, L. W., and Mauzerall, D. L.: Global health benefits of
682 mitigating ozone pollution with methane emission controls, *Proceedings of the National*
683 *Academy of Sciences of the United States of America*, 103, 3988,
684 <https://doi.org/10.1073/pnas.0600201103>, 2006.
- 685 Wiedinmyer, C., Akagi, S. K., Yokelson, R. J., Emmons, L. K., Al-Saadi, J. A., Orlando, J. J.,
686 and Soja, A. J.: The Fire INventory from NCAR (FINN): a high resolution global model
687 to estimate the emissions from open burning, *Geoscientific Model Development*, 4,
688 625–641, <https://doi.org/10.5194/gmd-4-625-2011>, 2011.
- 689 Wu, R. and Xie, S.: Spatial Distribution of Ozone Formation in China Derived from Emissions
690 of Speciated Volatile Organic Compounds, *Environ. Sci. Technol.*, 51, 2574–2583,
691 <https://doi.org/10.1021/acs.est.6b03634>, 2017.
- 692 Xue, T., Zheng, Y., Geng, G., Xiao, Q., Meng, X., Wang, M., Li, X., Wu, N., Zhang, Q., and
693 Zhu, T.: Estimating Spatiotemporal Variation in Ambient Ozone Exposure during
694 2013–2017 Using a Data-Fusion Model, *Environ. Sci. Technol.*, 54, 14877–14888,
695 <https://doi.org/10.1021/acs.est.0c03098>, 2020.
- 696 Yamaji, K., Ohara, T., Uno, I., Kurokawa, J., Pochanart, P., and Akimoto, H.: Future prediction
697 of surface ozone over east Asia using models-3 community multiscale air quality
698 modeling system and regional emission inventory in Asia, *Journal of Geophysical*
699 *Research: Atmospheres*, 113, 2008.
- 700 Yang, Z., Cheng, H. R., Wang, Z. W., Peng, J., Zhu, J. X., Lyu, X. P., and Guo, H.: Chemical
701 characteristics of atmospheric carbonyl compounds and source identification of
702 formaldehyde in Wuhan, Central China, *Atmospheric Research*, 228, 95–106,
703 <https://doi.org/10.1016/j.atmosres.2019.05.020>, 2019.
- 704 Zhang, H., Li, J., Ying, Q., Guven, B. B., and Olaguer, E. P.: Source apportionment of
705 formaldehyde during TexAQS 2006 using a source-oriented chemical transport model,
706 *Journal of Geophysical Research: Atmospheres*, 118, 1525–1535,
707 <https://doi.org/10.1002/jgrd.50197>, 2013.
- 708
- 709

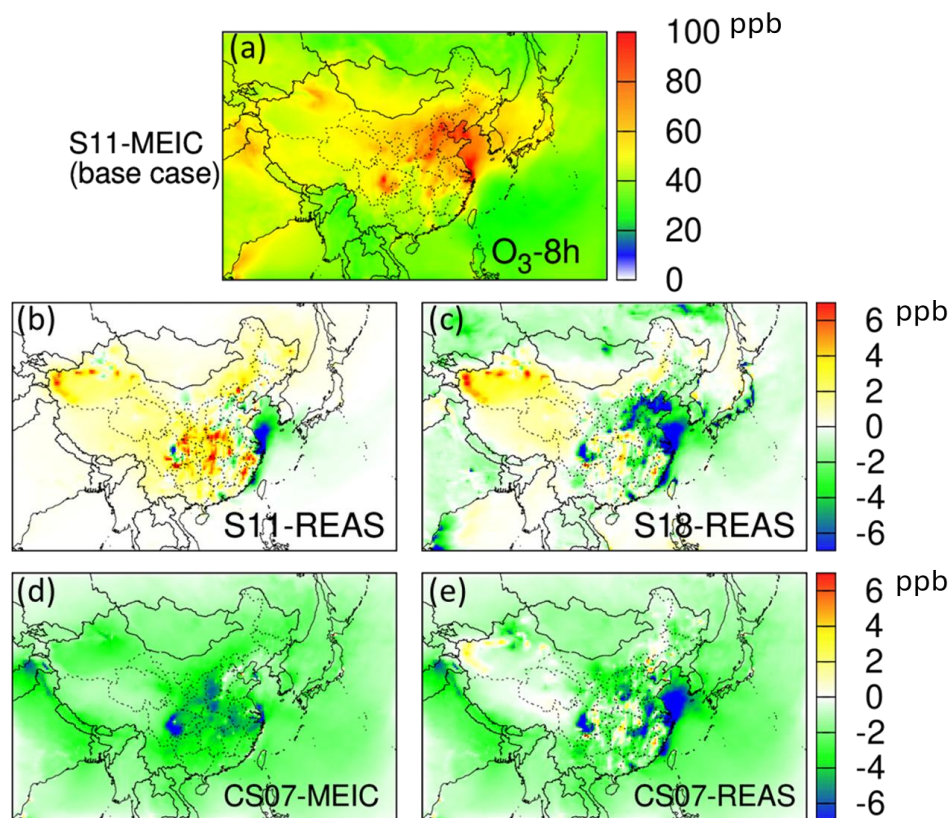


Figure 1. Predicted monthly averages of MDA8 O₃ (O₃-8h) concentrations in July 2017 using (a) the S11 mechanism and MEIC emission inventory (base case), and the differences between the base case and cases using alternative photochemical mechanisms and emission inventories (alternative case – base case): (b) S11 and REAS, (c) S18 and REAS, (d) CS07 and MEIC, and (e) CS07 and REAS inventories. Units are ppb.

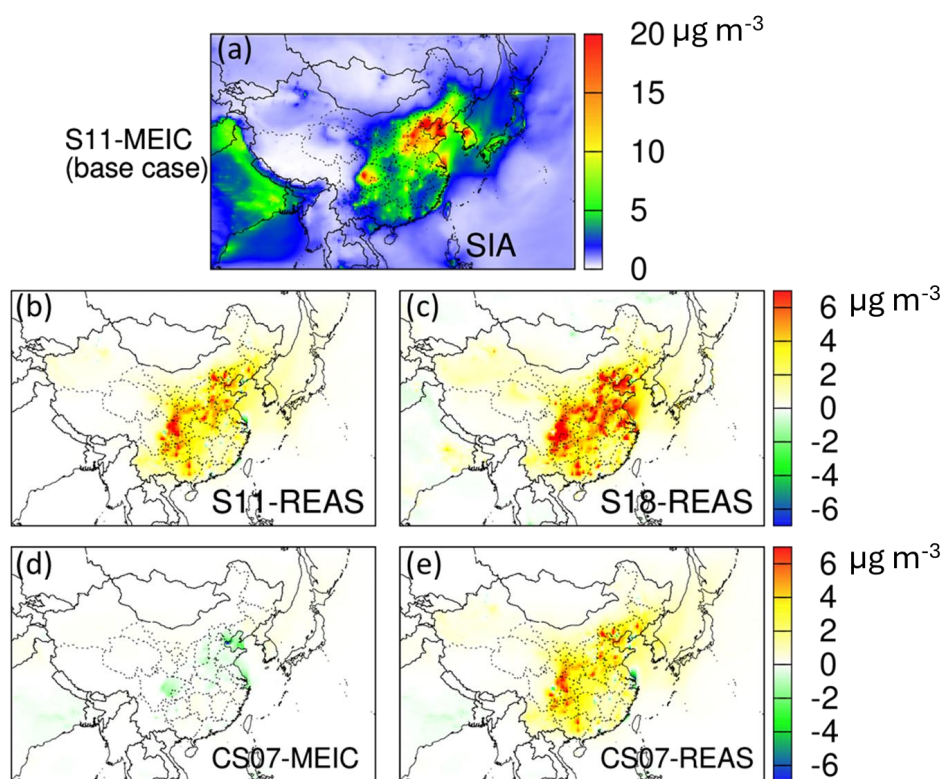
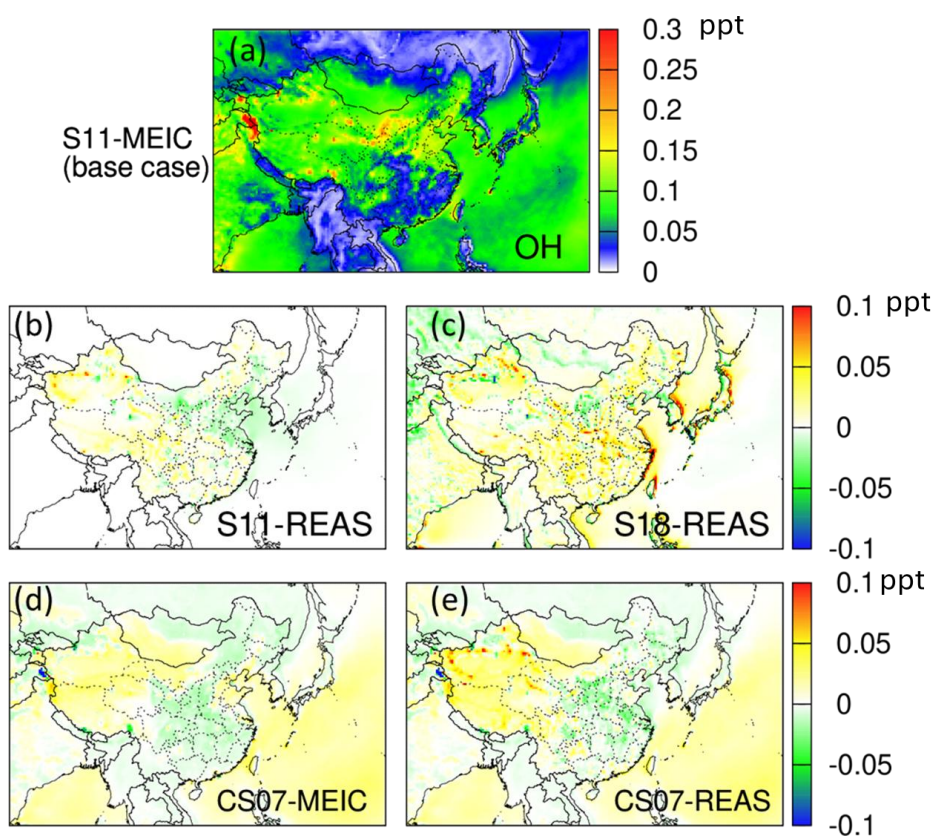


Figure 2. Predicted monthly averages of secondary inorganic aerosol (the sum of nitrate, sulfate and ammonium ion, SIA) concentrations in July 2017 using (a) the S11 mechanism and MEIC emission inventory (base case), and the differences between base case and cases using other photochemical mechanisms and emission inventories (alternative case – base case): (b) S11 and REAS, (c) S18 and REAS, (d) CS07 and MEIC, and (e) CS07 and REAS. Units are $\mu\text{g m}^{-3}$.



727



728

729

730 **Figure 3.** Predicted monthly averages of OH radical concentrations in July 2017 using (a) the
731 S11 mechanism and MEIC emission inventory (base case), and the differences between the
732 base case and cases using other photochemical mechanisms and emission inventories
733 (alternative case – base case): (b) S11 and REAS, (c) S18 and REAS, (d) CS07 and MEIC, and
734 (e) CS07 and REAS. Units are ppt. ($0.1 \text{ ppt} \sim 2.46 \times 10^6 \text{ molec cm}^{-3}$)

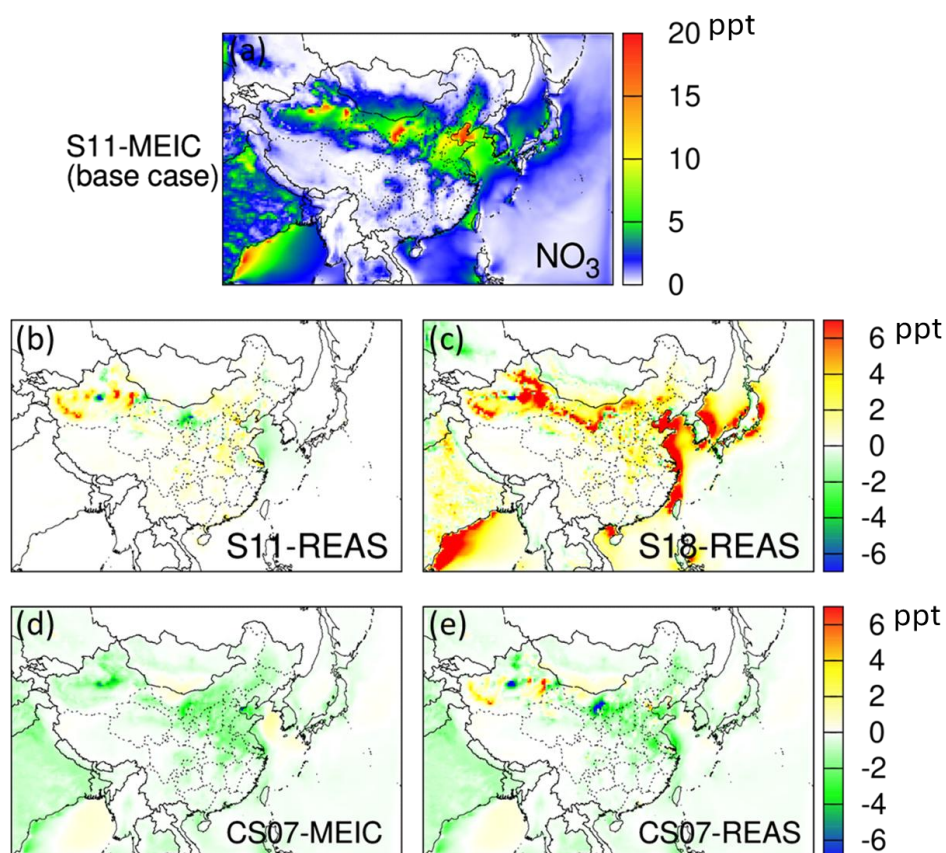
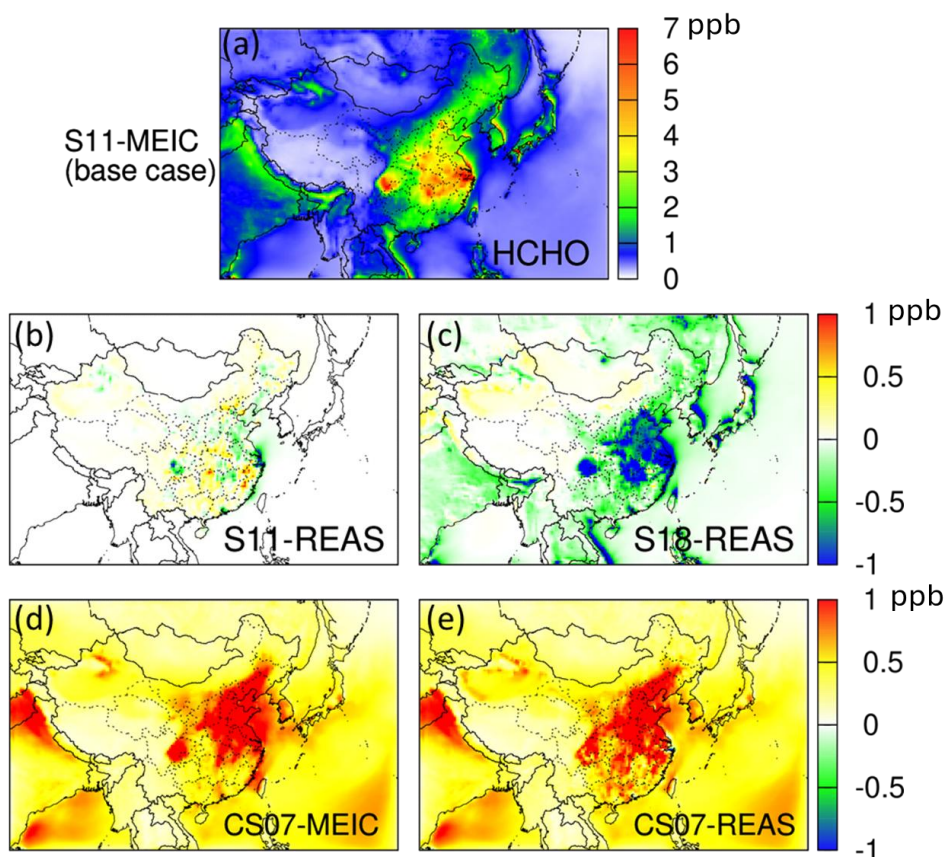


Figure 4. Predicted monthly averages of NO_3 radical concentrations in July 2017 using (a) the S11 mechanism and MEIC emission inventory (base case), and the differences between the base case and cases using alternative photochemical mechanisms and emission inventories (alternative case – base case): (b) S11 and REAS, (c) S18 and REAS, (d) CS07 and MEIC, and (e) CS07 and REAS. Units are in ppt. ($0.1 \text{ ppt} \sim 2.46 \times 10^6 \text{ molec cm}^{-3}$)



743

744 **Figure 5.** Predicted monthly averages of HCHO concentrations in July 2017 using (a) the S11
745 mechanism and MEIC emission inventory (base case), and the differences between the base
746 case and cases using alternative photochemical mechanisms and emission inventories
747 (alternative case – base case): (b) S11 and REAS, (c) S18 and REAS, (d) CS07 and MEIC, and
748 (e) CS07 and REAS. Units are ppb.



749

750

751

752

753

754

755

756

757

758

759

760

761

762

763

764

765

766

767

768

769

770

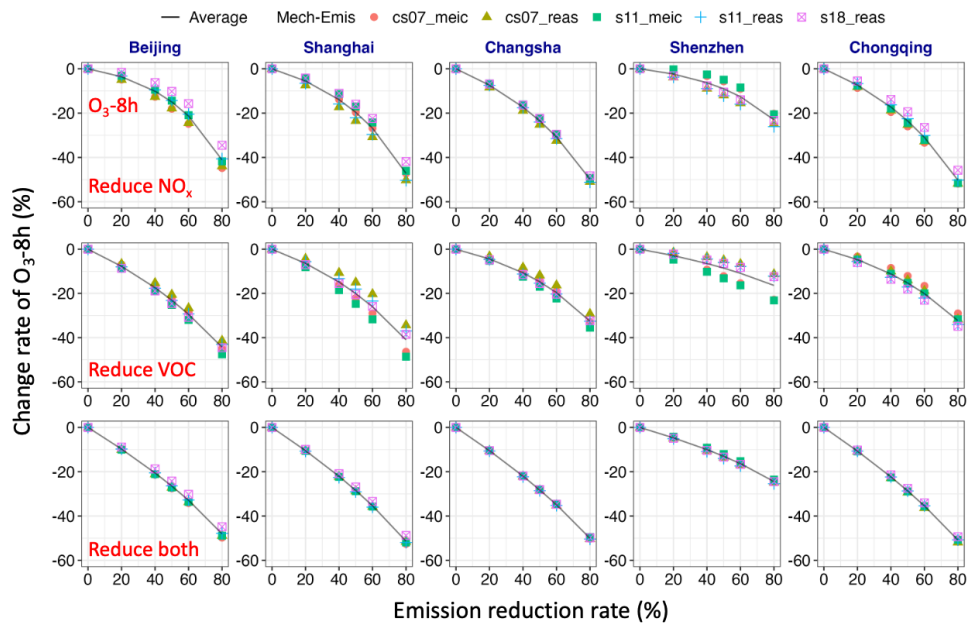


Figure 6. Predicted changes of monthly average MDA8 O₃ (O₃-8h) concentrations in July 2017 due to reductions of NO_x only (first row), VOCs only (second row), and NO_x and VOCs (third row) using different photochemical mechanisms and emission inventories. The black line represents the average change across all mechanisms and inventories at different levels of emission reductions.

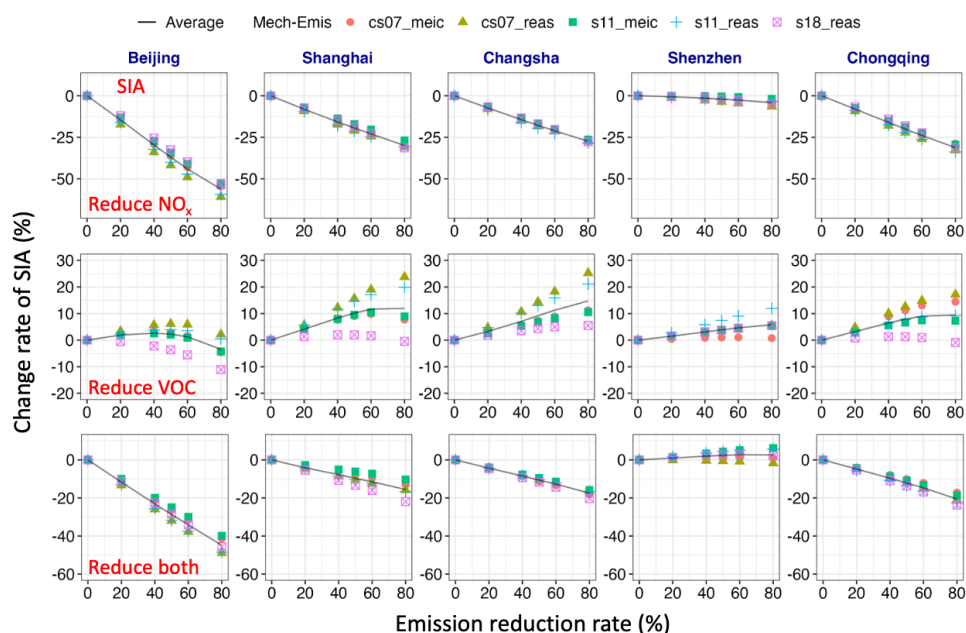


Figure 7. Predicted changes of monthly average secondary inorganic aerosol (SIA) concentrations in July 2017 due to reductions of NO_x only (first row), VOCs only (second row), and NO_x and VOCs (third row) using different photochemical mechanisms and emission inventories. The black line represents the average change across all mechanisms and inventories at different levels of emission reductions.

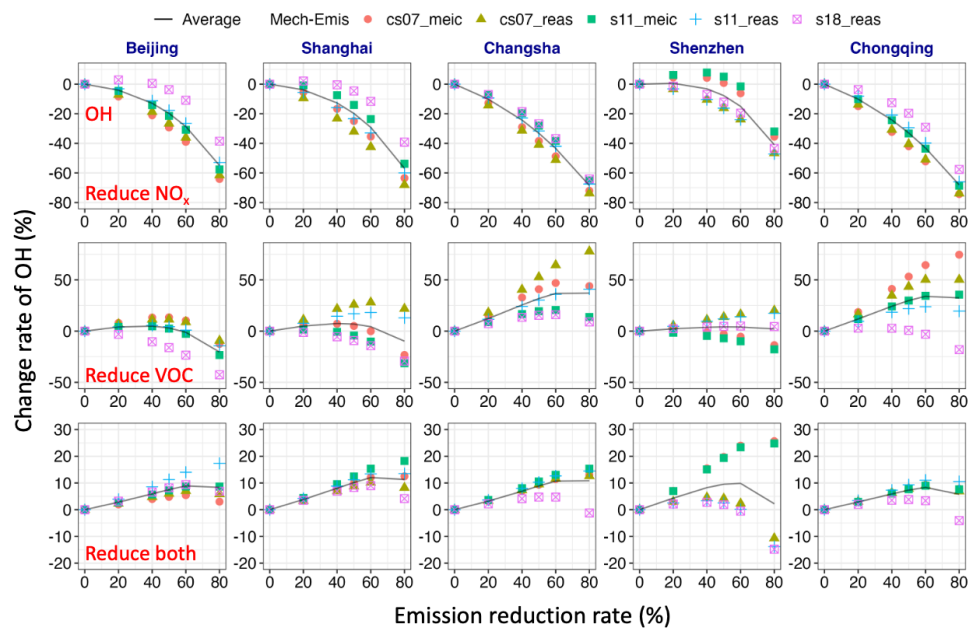


Figure 8. Predicted changes of monthly average OH radical concentrations in July 2025 due to reductions of NO_x only (first row), VOCs only (second row), and NO_x and VOCs (third row) using different photochemical mechanisms and emission inventories. The black line represents the average change across all mechanisms and inventories at different levels of emission reductions.

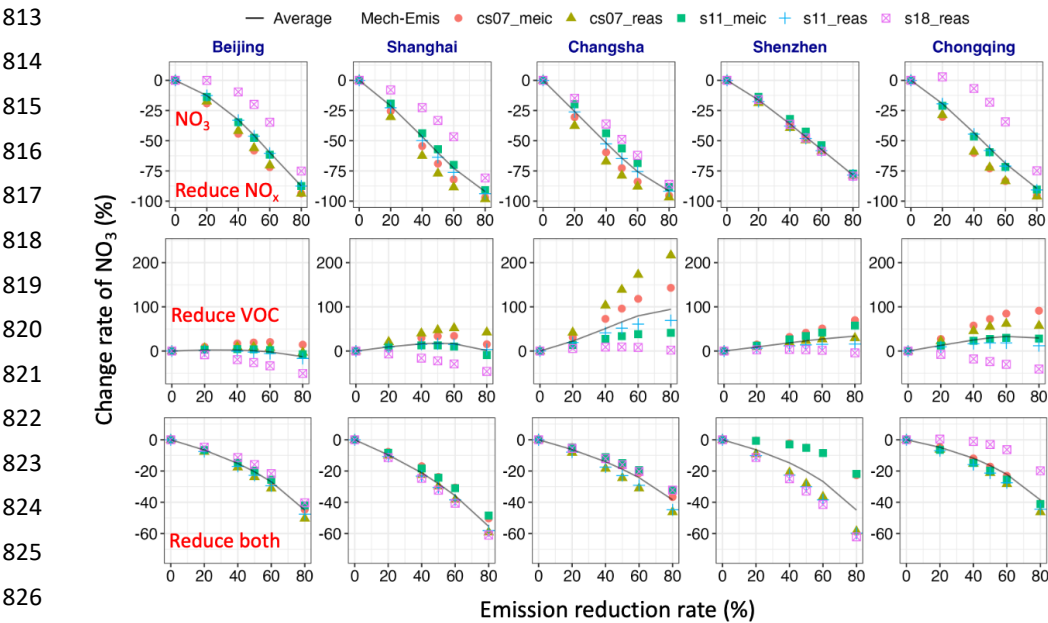


Figure 9. Predicted changes of monthly average NO_3 radical concentrations in July 2025 due to reductions of NO_x only (first row), VOCs only (second row), and NO_x and VOCs (third row) using different photochemical mechanisms and emission inventories. The black line represents the average change across all mechanisms and inventories at different levels of emission reductions.

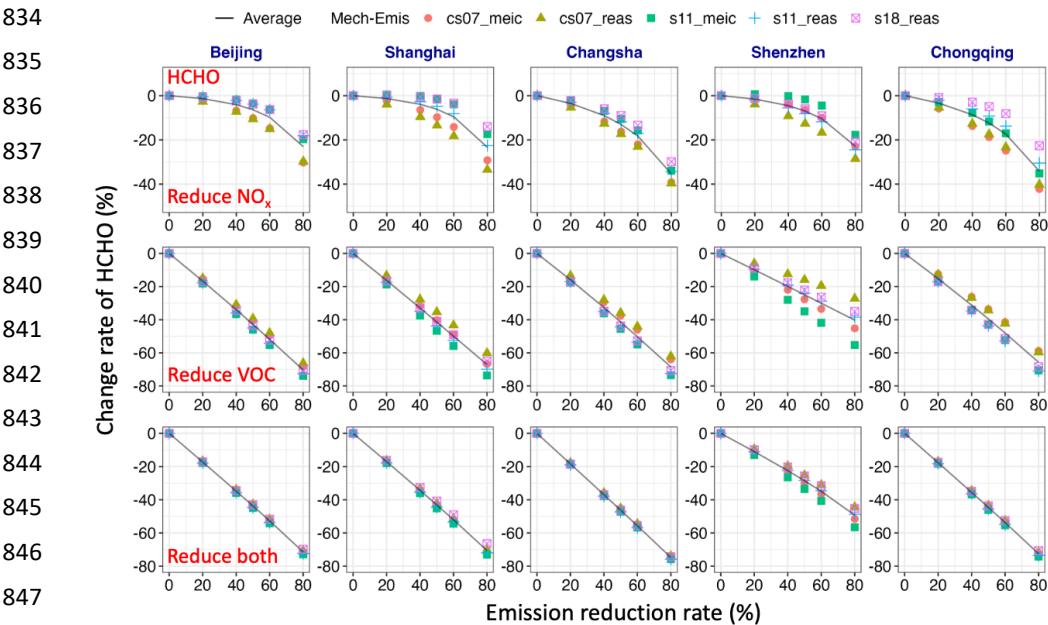


Figure 10. Predicted changes of monthly average HCHO concentrations in July 2025 due to reductions of NO_x only (first row), VOCs only (second row), and NO_x and VOCs (third row) using different photochemical mechanisms and emission inventories. The black line represents the average change across all mechanisms and inventories at different levels of emission reductions.